Nearly Perfect Polycrystalline, Large-Grained Silicon Arrays Formed at Low-Temperature Ambient by Local Pyrolysis

Jun Hee Choi,*,[†,§] Ho Young Ahn,[†] Yun Sung Lee,[†] Youn Taek Ryu,[‡] Kyung Sang Cho,[†] Sun Il Kim,[†] Chan Wook Baik,[†] Tae-Ho Kim,[†] Eun Hong Lee,[†] Hyobin Yoo,[§] Kunsu Kim,[§] Miyoung Kim,*,[§] and Jong Min Kim[†]

[†]Frontier Research Laboratory, Samsung Advanced Institute of Technology, Samsung Electronics, Yongin, Kyunggi-do 446-712, South Korea

[‡]Nano Fabrication Group, Samsung Advanced Institute of Technology, Samsung Electronics, Yongin, Kyunggi-do 446-712, South Korea

[§]Department of Materials Science and Engineering, Seoul National University, Seoul 151-744, South Korea

Ⓢ Supporting Information

ABSTRACT: We report low-temperature ambient synthesis of high-quality, several micrometer thick polycrystalline silicon arrays on soda lime glass substrates by local pyrolysis, where SiH_4 gas is locally decomposed near and condensed on the resistively heated microheater arrays with an average growth rate of 50 nm/s. The silicon arrays had nearly perfect crystallinity and a minimum grain size larger than 0.2 μm, as determined by spatially resolved Raman spectroscopy and transmission electron microscopy. Boron-doped silicon arrays by the local pyrolysis was further fabricated to yield concentric p-i-n heterojunction arrays with rectifying current−voltage or photovoltaic characteristics.
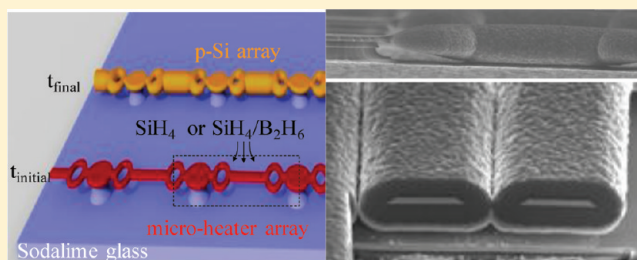
INTRODUCTION

There is no question that single crystal silicon is ideal for certain electronic applications, including solid-state opto-electronic devices such as optical modulators,[1] thin-film transistors (TFTs), and solar cells. Polycrystalline silicon (p-Si) has been intensively studied as an alternative for single crystal;[2,3] however, the crystalline quality of p-Si is still limited for formation on soda lime glass substrates (SLGS) because of the low glass processing temperature (upper limit of ∼550 °C). p-Si thermally grown at such low temperatures using low pressure chemical vapor deposition (LPCVD) results in low film quality.[4] Device-grade p-Si can be grown at even lower substrate temperatures (e.g., 300 °C) when using other energy sources such as plasma, hot wires, and lasers. Very-high-frequency-plasma-enhanced chemical vapor deposition[5] (VHF-PECVD) or hot-wire chemical vapor deposition[6] (HW-CVD) are actively developed to grow p-Si for solar cells. Another approach to make p-Si is excimer-laser[7] or electric-field[8] driven crystallization of amorphous silicon (a-Si),[9] used with TFTs in active matrix organic light-emitting diodes. Nevertheless, the poor crystallinity and small grain size must be overcome; these issues are critical for improved device performance. The conversion efficiency of solar cells and the field-effect mobility of TFTs are expected to be further enhanced by improving these parameters. Furthermore, the growth rate of p-Si formed by VHF-CVD, currently limited to 8 nm/s,[10] must be enhanced for higher throughput.

Local heating-based nanostructure formation has recently been reported.[11−16] The local heating was achieved through a single suspended microheater. We extended the single microheater into a microheater array (MHA), which can be resistively and locally heated up to 1200 °C even on a SLGS. It has been used to make carbon nanotubes[17] or semiconductor nanorods[18,19] and for fine patterning of organic layers.[20] Here, we report nearly perfect, large-grained (grain size > 0.2 μm) p-Si arrays on a SLGS by local pyrolysis, where SiH_4 gas is locally decomposed near and condensed on the resistively heated microheater arrays (MHAs) with a growth rate of 50 nm/s. Concentric p-i-n heterojunction arrays and their rectifying current−voltage or photovoltaic characteristics were further demonstrated.

EXPERIMENTAL SECTION

Fabrication and Design of the MHA. For local-heat-assisted pyrolysis (Figure 1), a local heating template was prepared by forming the MHA on a SLGS, as described in ref 17. Using PECVD and sputtering, 3 μm thick SiO_2 and 1 μm thick Mo layers, respectively, were successively deposited on a glass substrate. The MHA was formed through conventional photolithography followed by reactive ion etching of Mo using Cl_2/O_2 gas mixture and successive isotropic wet etching of the SiO_2 to form insulating columns and bridges
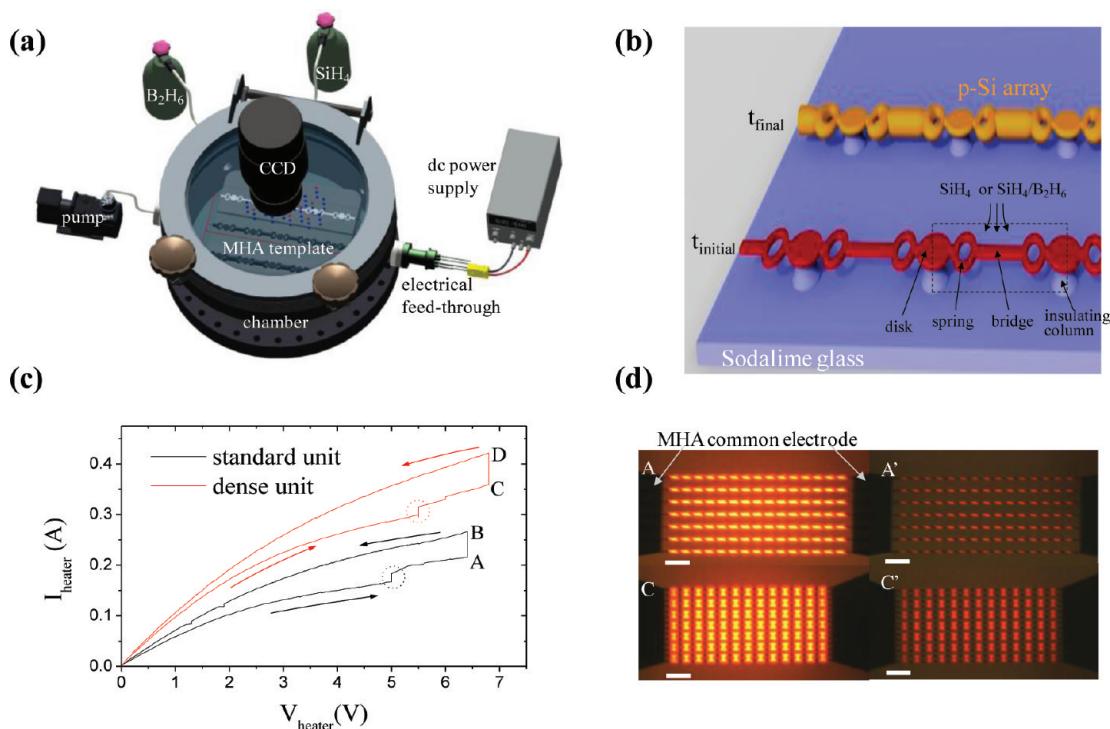
Figure 1. (a) Local pyrolysis growth system, (b) schematic diagram showing growth of intrinsic or p-type p-Si arrays by local pyrolysis reaction of SiH$_4$ or SiH$_4$/B$_2$H$_6$ (the dotted rectangle represents the microheater unit), (c) I−V curves of MHAs with standard and dense units for resistive heating (the dashed circles represent resistance change by annealing effect), and (d) corresponding CCD images of glowing MHAs at conditions A and C in panel c. A′ and C′ are the corresponding glow images of A and C, ∼10 s after the local pyrolysis started. Scale bars in panel d are 330 μm.

(Figure 1b). The MHA had a repeating heater unit. Two different types of heater units, called standard and dense units, were used to grow the p-Si array. The standard unit (Figure 2a−c) consisted of a major bridge, each end of which was connected to a ring-shaped spring (stress-releasing damper) and a circular disk supported by an insulating column. The dense unit (Figure 2d,e, and lower panel of Figure 4a) consisted of two parallel major bridges, whose end connections were the same as those of the standard unit except that there were two springs connected to each end; three minor bridges were connected between the major bridges. The ring-shaped springs were designed to relax thermal stresses and to prevent the breakage of the bridge during a heating cycle. The length and width of the major bridge in the standard unit were 50 and 10 μm (70 and 10 μm in the dense unit), respectively, while those of the minor bridge in the dense unit were 7 and 60 μm, respectively. The inner and outer diameters of the ring-shaped spring were 18 and 26 μm, respectively. The diameter of the metallic disk supported by the insulating column was 30 μm in the standard unit (20 μm in the dense unit). Heater units (15 for the standard unit, 13 for the dense unit) were connected in series (*x*-direction). These serially connected units were also propagated in parallel (*y*-direction) between the two common electrodes. The number of parallel connections was 14 and 7 for the standard and the dense heater units, respectively.

p-Si Synthesis by Local Pyrolysis. The MHA template was placed within a chamber equipped with a charge-coupled device (CCD) and connected to an exterior dc power supply through an electrical feed-through (Figure 1b). The chamber was evacuated at room temperature to 7.5×10^{-3} Torr. Thermal cycling for the local pyrolysis is detailed in Figure 1c. The MHA with the standard unit was resistively heated under a dc bias (V_{heater}) of 5.0 V with a ramping rate of 0.1 V/s, then annealed for 2 min, during which time the current (I_{heater}) was increased from 165 to 185 mA, as indicated by the black dashed circle. Then, the V_{heater} was increased to 6.5 V (marked by A in Figure 1c). A gas mixture of 1000 sccm SiH$_4$ was then injected for 1 min to grow intrinsic p-Si. During the growth step (A to B marked in Figure 1c), the I_{heater} was increased from 214 to 266 mA. Finally, the

V_{heater} was decreased to 0 V at a rate of 0.05 V/s. For the dense unit, the cycling process was basically the same except that the first V_{heater} and I_{heater} values for annealing were 5.5 V and 295−318 mA (black dashed circles in Figure 1c), and the values for boron-doped p-Si growth (with a gas mixture of 1000 sccm SiH$_4$ and/or 100 sccm B$_2$H$_6$ (0.5% diluted in H$_2$)) were 6.8 V and 359−421 mA (C to D marked in Figure 1c), respectively. The full detailed explanation of the p-Si pyrolysis with I_{heater} vs time and V_{heater} vs time curves for the dense heater unit is described in the Supporting Information (Figure S1).

Estimating Crystallinity of p-Si. The crystallinity and the stress level of the p-Si on the MHA of the standard unit were investigated by micro-Raman spectroscopy with a 488 nm excitation wavelength. The detailed morphology of the p-Si array, including grain size and crystallinity, was investigated using high-resolution transmission electron microscopy (HR-TEM). For the TEM observations, the p-Si on the MHA was cross-sectionally milled using a focused gallium ion beam.

Fabrication and Electrical/Photovoltaic Characterization of p-i-n Heterojunction. The concentric p−i−n heterojunction was formed by successive deposition of intrinsic (50 nm) and n-type phosphorus-doped (50 nm) amorphous silicon (a-Si) layers around the boron-doped p-Si arrays using conventional PECVD at 250 °C with an RF power of 75 W. Because of an excellent step coverage of PECVD layers, a-Si layers were uniformly coated around the p-Si arrays (Figure 4a,b). The gas mixture was 1000 sccm SiH$_4$ (5% diluted in H$_2$) for the intrinsic layer and 500 sccm SiH$_4$ (5% diluted in H$_2$) with 500 sccm PH$_3$ (1% diluted in H$_2$) for the n-type layer. Aluminum (2.1 μm) or ITO (0.3 μm) layers were evaporated or sputtered through the shadow mask closing the common heater of the MHA. This procedure simultaneously formed the shell electrodes, the bottom common electrode, and electrical connection among them (Figure 4a). The core electrode was electrically connected to the common electrode of the MHA, and the shell electrode to the bottom common electrode. The I−V curves were measured between these two common electrodes. The illuminated I−V curves were obtained under the AM1.5 condition.
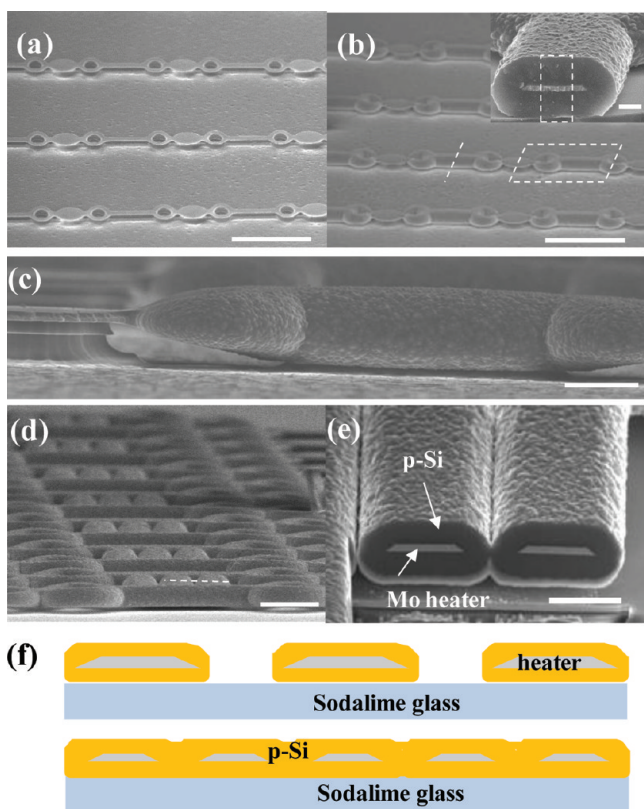
Figure 2. Scanning transmission microscopy images showing the p-Si growth with the standard unit (a−c) and the dense unit (d,e). Panels a and b−e show MHAs before and after p-Si formation, respectively. Inset of panel b is the cross-section of a dashed line in panel b. (c) Magnified image of the dashed parallelogram in panel b. (e) Cross-section of the dashed line in panel d. (f) Types of synthesized p-Si: an array (upper panel) or a film (lower panel) depending on thickness and heater spacing. Scale bars are 100 μm in panels a and b; 5 μm in the inset of panel b; 20 μm in panel c; 25 μm in panel d; 7 μm in e.

■ RESULTS AND DISCUSSION

Local Pyrolysis of p-Si Arrays. The p-Si arrays were formed at low-temperature ambient using local heat-assisted pyrolysis as schematically shown in Figure 1a,b. The measured substrate temperature by thermocouple was 70−80 °C. Local heating was achieved utilizing the molybdenum (Mo) MHA. When SiH_4 gas was exposed to the high-temperature surface of the MHA, it decomposed into chemically active radicals such as SiH_3, SiH_2, and SiH. These radicals then deposited as intrinsic p-Si around the MHA. Similarly, P-type p-Si arrays were formed using a SiH_4/B_2H_6 gas mixture (Figure 1b). The decomposition reaction is similar to that occurring near the tungsten filament in HW-CVD.[21,22] The major distinction is the heater temperature. In HW-CVD, the filament heater temperature (typically above 1300 °C) is so high that decomposed radicals are evaporated away from the filament and deposited onto a substrate separated by a few tens of centimeters. However, the heater temperature of the MHA in this experiment was maintained below 1000 °C. In this temperature regime, the decomposed radicals preferentially condense directly around the circumference of the MHA.

Figure 1c shows I_{heater}−V_{heater} curves for MHAs in the local pyrolysis. During heating (from V_{heater} = 0 to A or C in Figure 1c), the slope of the curve decreased with increasing V_{heater}, meaning that the electrical resistance (V_{heater}/I_{heater}) of the

MHA increased with temperature, as is typical for metals . When the V_{heater} exceeded a critical value, the I_{heater} increased with time even under a fixed V_{heater} (marked by dotted circles in Figure 1c). This is because the microstructure of the Mo heater changed above the critical temperature, resulting in better crystallinity and a larger grain size, and therefore lowered resistance. In the pyrolysis step (introduction of SiH_4 and/or B_2H_6 mixture of gases), at a different fixed V_{heater}, I_{heater} again increased from A to B and from C to D in Figure 1c, indicating p-Si growth around the MHA. This is explained by the increased volume during the growth and consequently a lower heater temperature under the fixed V_{heater}. This in turn yielded a lower electrical resistance and a higher I_{heater}. It should be noted that the initial glowing intensity of MHAs (A or C in Figure 1d) was abruptly decreased to the state (A′or C′ in Figure 1d) ∼10 s after the pyrolysis reaction started. This means that a substantial amount of p-Si is formed around the MHA during the initial pyrolysis stage.

The suspended Mo microheater unit had local temperature gradients that depended on the heating volume and the amount of heat transferred to the substrate. In the present heater unit (marked by the dotted rectangle in Figure 1b), the local temperature increased in the order of disk, spring, and bridge because of an increasing amount of resistive heating; the heat transfer to the substrate through the supporting insulating column followed the same order. The growth temperature in the bridge can be obtained by real-time fitting of the measured incandescent spectra with the blackbody emission.[23] When the microheater units were extended to the MHA, the temperature distribution was repeated across the MHA (Figure 1d). The range of temperature variation could be modulated by changing the relative dimensions of the bridge, spring, and disk as well as the location of the insulating column. The MHA structure with reduced temperature distribution is under investigation (see Supporting Information, Figure S2).

p-Si Array Morphology. Figure 2a shows the morphologies of the as-made MHA (standard unit) and Figure 2b,c shows the p-Si array after the pyrolysis reaction was completed. The growth of p-Si was omni-directional (inset of Figure 2b) around the microheater surface, revealing that the decomposition and growth reactions were uniform around the cross-sectional heater surface. The maximum p-Si thickness in the bridge region was ∼6.5 μm. Although the instantaneous growth rate, at constant V_{heater}, should decrease due to temperature decrease during p-Si growth, the average growth rate was 50 nm/s, much higher than that with other deposition methods.[10] Such a high growth rate may be due to localization of decomposed radicals such as SiH, SiH_2, and SiH_3 near the microheater surface. Increased radical concentration could facilitate the deposition reaction. The rough surface morphology observed in the inset of Figure 2b and Figure 2c indicates that the p-Si had a columnar structure in which the size of the protrusions was approximately the same as the planar grain size of p-Si, i.e., ranging from 0.25 to 0.75 μm. The p-Si thickness abruptly decreased in the transition from the spring to the disk and eventually the thickness in the disk region became less than 1 μm (Figure 2c). This thickness variation resulted from the temperature distribution as described above. The same trend in thickness variation also occurred for the MHA having a dense unit (Figure 2d,e). As illustrated in Figure 2f, synthesized p-Si can have the form of an array (upper panel) or a film (lower panel) depending on its thickness and the heater spacing. The

latter implies that the local pyrolysis reaction could be used for applications requiring a relatively large coverage of p-Si.

p-Si Array Crystallinity. Transmission electron microscopy (TEM) was carried out at position 1 of Figure 2c to further study the p-Si crystallinity. The cross-sectional views on the upper and lower sides of the Mo microheater bridge show the columnar morphology (Figure 3a,b). A typical crystalline
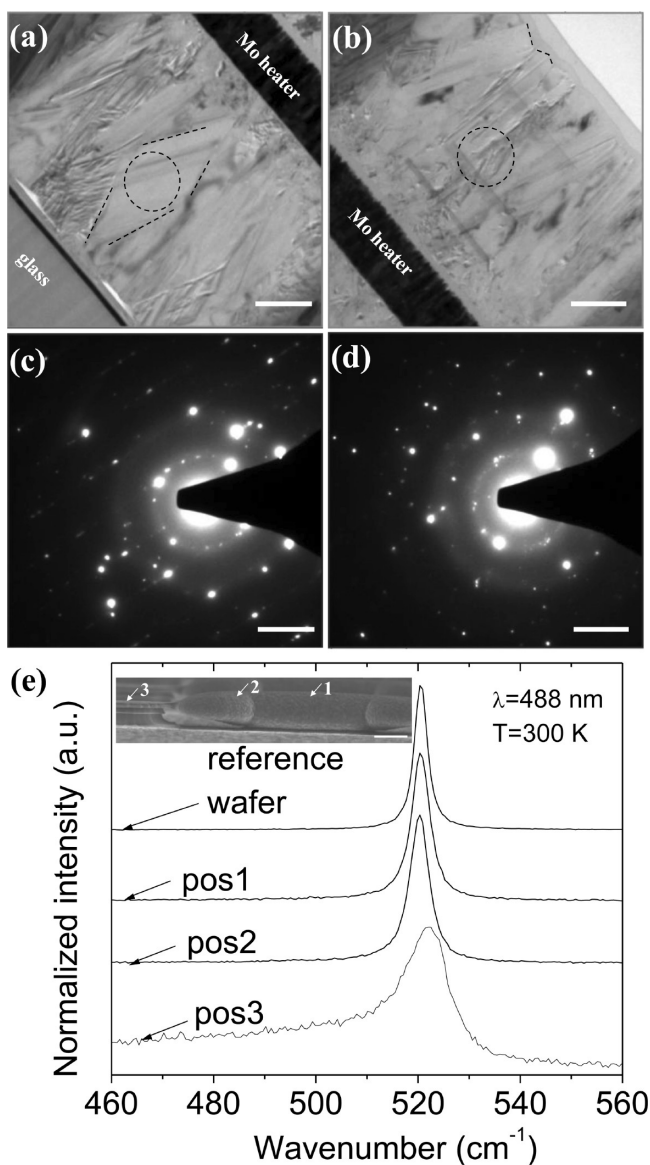
Figure 3. Bright field TEM images of the p-Si on the (a) lower and (b) upper side of the Mo microheater marked by a dotted rectangle in the inset of Figure 2b. (c,d) Diffraction patterns of the areas marked by dotted circles in panels a and b, respectively. (e) micro-Raman spectra at three different locations marked in inset redrawn from Figure 2c. Scale bars in panels a−d are 1 μm.

column is outlined by a dotted line in Figure 3a. The average size was greater than 2 μm in the direction perpendicular to the heater surface and greater than 0.2 μm in the parallel direction. The column or grain size was larger than that grown using other methods (typically less than 0.1 μm[24,25]). The surface morphology outlined by the dotted lines in Figure 3b is consistent with the rough surfaces shown in Figure 2c,e. The columnar morphology may have originated from the concentric

temperature gradient, which would have provided a concentration gradient of decomposed radicals around the heater surface. The vertical current flow is subject to less grain boundary scattering in this columnar structure. The electron diffraction patterns of a cross-sectional sample (Figure 3c,d) obtained from a selected area of 1 μm in diameter, marked by dotted circles in Figure 3a,b, consisted of regular peaks. The ring-shaped diffraction patterns typically observed in p-Si were not found, but only very weak additional peaks were observed. Such diffraction patterns confirm that the p-Si had an excellent crystallinity with a large grain size. We suggest that the decomposed radicals were so localized near the MHA that they were sufficiently energetic to form highly crystalline, large grain p-Si. However, the small grain region near the heater surface marked in Figure 3a,b indicates that initial nucleation was inhomogeneous.

The optical properties of the p-Si were examined by micro-Raman spectroscopy. Figure 3e shows the micro-Raman spectra of a p-Si array at three different locations noted in the inset redrawn from Figure 2c. The full-width at half-maximum (fwhm) and the stress induced wavenumber shift ($\Delta\omega$) of the optical-phonon mode were estimated by fitting a Lorentzian function to the spectra. At locations 1 and 2, the material appeared completely crystalline (peak at about 520 cm^{-1}), with no bands corresponding to amorphous material (peak at about 480 cm^{-1}). The fwhm at these locations were 4.2 and 4.4 cm^{-1}, respectively. These values are comparable to the measured one (3.6 cm^{-1}) for reference single crystalline Si (c-Si), proving a low defect density of p-Si in these regions. In addition, the peak wavenumbers (ω_p) at positions 1 and 2 were 520.5 and 520.3 cm^{-1}, respectively, whereas the peak value (ω_c) of the reference c-Si was 520.5 cm^{-1}. This means that the stress calculated using the following equation[26] is also quite low.

$$\sigma(\text{MPa}) = -250\Delta\omega(\text{cm}^{-1}) \qquad (1)$$

where $\Delta\omega = \omega_p - \omega_c$.

The p-Si crystals at locations 1 and 2 were nearly stress-free (~0 MPa) and slightly tensile-stressed (~50 MPa), respectively. These small fwhm and $\Delta\omega$ values again indicate that the crystallinity of p-Si in these locations was much higher than that reported by other methods such as excimer laser crystallization of a-Si.[18] The spectrum for position 3, however, exhibited an asymmetric and wide peak. This made it difficult to obtain reliable fwhm and $\Delta\omega$ values by simple fitting of a single Lorentzian function. The amorphous band around 480 cm^{-1} was absent. In this region, the crystallinity was not high even though the amorphous fraction was negligible. The variation in the crystallinity of p-Si can be explained by the temperature variation in the microheater unit, as described earlier. By direct comparison with the fwhm and $\Delta\omega$ from low-temperature chemical vapor deposition, the temperature of the MHA at positions 1 and 2 was estimated to be about 900 °C.[27]

Concentric p-i-n Heterojunction Based on Boron-Doped p-Si Arrays. Concentric p-i-n heterojunction diode arrays were fabricated to measure electrical properties of p-Si grown around the MHA with dense unit, as schematically shown in the upper panel of Figure 4a. The diode structure was comprised of p-Si (p-type)/amorphous silicon (a-Si, i-type)/a-Si (n-type)/Al or indium tin oxide (ITO) layers (the shell electrode) concentrically formed around the Mo microheater (the core electrode) (Figure 4b). Dark or illuminated I−V measurements of the structure were performed between these core and shell electrodes (upper panel of Figure 4a). With the
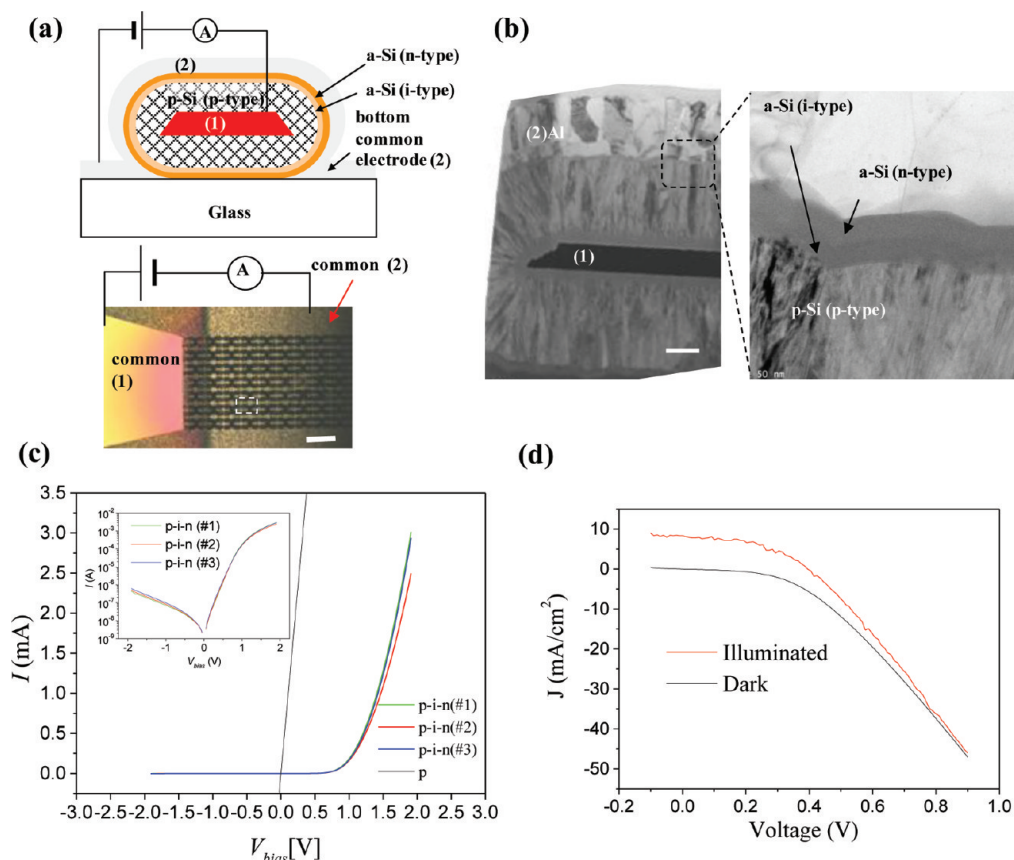
Figure 4. (a) Schematic of p-i-n heterojunction diode (upper panel) and its corresponding optical microscope image (lower panel), (b) bright field, cross-sectional TEM images of the heterojunction, (c) dark $I-V$ curves of the p-Si (straight line) and the p-i-n heterojunction with the Al shell electrode. (Inset of panel c) Log $I-V$ plot of the p-i-n structure. (d) Dark and illuminated $I-V$ curves with the ITO shell electrode under the AM 1.5 condition. In panels a and b, (1) represents Mo microheater core electrode, common (1) represents the common electrode of the core electrodes (1); (2) represents Al or ITO shell electrode, and common (2) represents the common electrode of the shell electrodes (2). Scale bars in the lower panel of a, the left panel of b, and the right panel of b are 300, 1, and 0.05 μm, respectively.

Al shell electrode, the diode exhibits clear rectification, with average forward-to-reverse current ratios at $\pm$1.1 and 1.9 V of 3.18×10^3 and 1.70×10^4, respectively (Figure 4c). From this diode characteristic, it can be seen that p-type doping was successfully achieved in the local pyrolysis simply by introducing boron containing source gas. The p-i-n junction was also utilized with the ITO shell electrode to make solar cells. Figure 4d shows the dark and illuminated $I-V$ curves under AM1.5 equivalent conditions. The solar cell typically showed an open circuit voltage (V_{oc}) of 0.40 V, a fill factor (FF) of 47%, and an efficiency of 1.8%. The described variation in thickness and crystallinity of the p-Si array, as well as the high series resistance, appears to limit the efficiency.

CONCLUSIONS

In conclusion, several micrometers thick, nearly perfect, large grained (grain size > 0.2 μm) p-Si arrays were successfully grown with a high growth rate of 50 nm/s at low-temperature ambient by a novel method, local pyrolysis reaction. The temperature limitation of a SLGS was overcome by the local pyrolysis. The concentric p-i-n heterojunction diode structure yielded a forward to reverse current ratio of 1.70×10^4 at $\pm$1.9 V, meaning successful p-type doping is also available using this method. This approach and thus potential applications[28] will benefit from a uniform temperature microheater design and improved low-resistance metallization process.

ASSOCIATED CONTENT

Ⓢ Supporting Information

I_{heater}−time and V_{heater}−time curves; new microheater design. This material is available free of charge via the Internet at http://pubs.acs.org.

AUTHOR INFORMATION

Corresponding Author

* E-mail: joonie.choi@samsung.com (J.H.C.); mkim@snu.ac.kr (M.K.).

Notes

The authors declare no competing financial interest.

ACKNOWLEDGMENTS

REFERENCES

(1) Liu, A.; Jones, R.; Liao, L.; Rubio, D.; Rubin, D.; Cohen, O.; Nicolaescu, R.; Paniccia, M. *Nature* **2004**, *427*, 615−618.

(2) Kalihai, V.; Tadmor, E. B.; Haugstad, G.; Frisbie, C. D. *Adv. Mater.* **2008**, *20*, 4033−4039.

(3) Findikoglu, A. T.; Choi, W.; Matias, V.; Holesinger, T. G.; Jia, Q. X.; Peterson, D. E. *Adv. Mater.* **2005**, *17*, 1527−1531.

(4) Harbeke, G.; Krausbauer, L.; Steigmeier, E. F.; Widmer, A. E.; Kappert, H. F.; Neugebauer, G. *J. Electrochem. Soc.* **1984**, *131*, 675−682.

(5) Parascandolo, G.; Bugnon, G.; Feltrin, A.; Ballif, C. *Prog. Photovoltaics* **2010**, *18*, 257−264.

(6) Lien, S. Y.; Mao, H. Y.; Wu, B. R.; Horng, R. H.; Wuu, D. S. *Chem. Vap. Deposition* **2007**, *13*, 247−252.

(7) Delmdahl, R. *Nat. Photonics* **2010**, *4*, 286−287.

(8) Jang, J.; Oh, J. Y.; Kim, S. K.; Choi, Y. J.; Yoon, S. Y.; Kim, C. O. *Nature* **1998**, *395*, 481−483.

(9) Sharma, K.; Branca, A.; Illiberi, A.; Tichelaar, F. D.; Creatore, M.; van de Sanden, M. C. M. *Adv. Energy Mater.* **2011**, *1*, 401−406.

(10) Sobajima, Y.; Nishino, M.; Fukumori, T.; Kurihara, M.; Higuchi, T.; Nakano, S.; Toyama, T.; Okamoto, H. *Sol. Energy Mater. Sol. Cells* **2009**, *93*, 980−983.

(11) Englander, O.; Christensen, D.; Lin, L. *Appl. Phys. Lett.* **2003**, *82*, 4797−4799.

(12) Englander, O.; Christensen, D.; Kim, J.; Lin, L.; Morris, S. J. S. *Nano Lett.* **2005**, *5*, 705−708.

(13) Kawano, T.; Christensen, D.; Chen, S.; Cho, C. Y.; Lin, L. *Appl. Phys. Lett.* **2006**, *89*, 163510.

(14) Dittmer, S.; Mudgal, S.; Nerushev, O. A.; Campbell, E. E. B. *Low Temp. Phys.* **2008**, *34*, 834−837.

(15) Sosnowchik, B. D.; Lin, L.; Englander, O. *J. Appl. Phys.* **2010**, *107*, 051101.

(16) Engstrøm, D. S.; Rupesinghe, N. L.; Teo, K. B. K.; Milne, W. I.; Bøgild, P. *J. Micromech. Microeng.* **2011**, *21*, 015004.

(17) Kim, D. Y.; Choi, J. H.; Zoulkarneev, A. R.; Yang, M. H.; Han, I. T.; Kim, H. J.; Kim, S. I.; Baik, C. W.; Park, J. H.; Yoo, J. B.; Kim, J. M. *IEEE Electron Device Lett.* **2009**, *30*, 709−711.

(18) Kim, Y. J.; Jeon, J. M.; Choi, J. H.; Park, S. S.; Kim, S. I.; Baik, C. W.; Kim, M.; Kim, J. M.; Yi, G. C. *Nanotechnology* **2010**, *21*, 265603.

(19) Hong, Y. J.; Kim, Y. J.; Jeon, J. M.; Kim, M.; Choi, J. H.; Baik, C. W.; Kim, S. I.; Park, S. S.; Kim, J. M.; Yi, G. C. *Nanotechnology* **2011**, *22*, 205602.

(20) Choi, J. H.; Zoulkarneev, A.; Noh, T. Y.; Lee, Y. G.; Kim, S. I.; Park, S. S.; Baik, C. W.; Choi, B. L.; Kim, M.; Yi, G. C.; Kim, J. M. *J. Vac. Sci. Technol., B* **2011**, *29*, 021016.

(21) Doyle, J.; Robertson, R.; Lin, G. H.; He, M. Z.; Gallagher, A. *J. Appl. Phys.* **1988**, *64*, 3215−3223.

(22) Chen, X.; Xu, J.; Wang, R. M.; Yu, D. *Adv. Mater.* **2003**, *15*, 419−421.

(23) Li, P.; Jiang, K. L.; Liu, M.; Li, Q. Q.; Fan, S. S.; Sun, J. L. *Appl. Phys. Lett.* **2003**, *82*, 1763−1765.

(24) Finger, F.; Hapke, P.; Luysberg, M.; Carius, R.; Wagner, H.; Scheib, M. *Appl. Phys. Lett.* **1994**, *65*, 2588−2590.

(25) Kondo, M. *Sol. Energy Mater. Sol. Cells* **2003**, *78*, 543−566.

(26) Kitahara, K.; Yamazaki, R.; Kurosawa, T.; Nakajima, K.; Moritani, A. *Jpn. J. Appl. Phys.* **2002**, *41*, 5055−5057.

(27) Teixeira, R. C.; Doi, I.; Zakia, M. B. P.; Diniz, J. A.; Swart, J. W. *Mater. Sci. Eng. B* **2004**, *112*, 160−164.

(28) Choi, J. H.; Zoulkarneev, A.; Kim, S. I.; Baik, C. W.; Yang, M. H.; Park, S. S.; Suh, H.; Kim, U. J.; Son, H. B.; Lee, J. S.; Kim, M.; Kim, J. M.; Kim, K. *Nat. Photonics* **2011**, *5*, 763−769.

2477

dx.doi.org/10.1021/cg3001015 | *Cryst. Growth Des.* 2012, 12, 2472−2477